JOURNAL OF COMPUTATIONAL PHYSICS 90, 458–485 (1990)

A Comparison of First and Second Order Rezoned and Lagrangian Godunov Solutions*

M. S. HALL

3102 Waterside Lane, Alexandria, Virginia 22309

Received December 20, 1988; revised June 7, 1989

In this paper we present solutions from a Godunov-type algorithm to a selection of hydrodynamics test problems. Included in this selection are: implosions in planar, cylindrical, and spherical coordinates, piston problems with a variety of mesh configurations including the difficult Saltzman problem, interacting blast waves, and a spherical expansion on a rectangular mesh. These solutions have been obtained using CAVEAT, a three-dimensional arbitrary Lagrangian/Eulerian (ALE) hydrodynamics code that employs a Godunov method of solution with an approximate Riemann solver. First- and second-order solutions are presented for most of the problems and rezoned and Lagrangian solutions to the implosion (Noh) problem are compared. © 1990 Academic Press, Inc.

INTRODUCTION

In this paper we present solutions from a Godunov-type algorithm to a selection of hydrodynamics test problems in which strong shocks occur. The test problems chosen have recently appeared in the literature or are considered to be standard test problems for hydrodynamics codes used at Lawrence Livermore National Laboratory and elsewhere. The purpose of this paper is to demonstrate the effectiveness and usefulness of the method when applied to problems involving a variety of computational difficulties including uneven mesh spacing, non-rectangular zones, oblique shocks, and complicated interactions of multiple shocks. For the purpose of comparing these results with results generated using other methods, wherever possible we use the same mesh spacing, initial conditions, and boundary conditions as have been used by others attempting to solve the same problems. We have not attempted to prove convergence by such techniques as mesh refinement. The method is in fact only as accurate as is the approximation to the equation of state used in the Riemann solver, and thus in application accuracy of the results depends on more than mesh size.

In the Godunov approach all variables are assumed to be constant (first-order method) or linear (second-order method) within a computational cell. This results

* This work was performed under the auspices of the U.S. Department of Energy by the Lawrence Livermore National Laboratory under Contract W-7405-Eng-48.

0021-9991/90 $3.00

in discontinuities throughout the mesh, which are resolved by solving a Riemann shock-tube problem corresponding to each cell face. This solution describes the shock wave, rarefaction wave, and contact discontinuity resulting from a discontinuity in one or more of the primary variables in a one-dimensional flow field. The cell face corresponds to the contact discontinuity, across which the density and internal energy can change but the velocity and pressure do not. The cell face then moves with the velocity of the contact discontinuity, and the solution is advanced in time using a conservative advection scheme. The approximate, non-iterative Riemann solver employed in the code was developed by J. Dukowicz [1], and is based on the two-shock approximation in which the rarefaction that develops as a result of the discontinuity is treated as a weak shock. This method is by its very nature well-suited to solving problems in which an actual discontinuity in the flow field exists, and the result is good resolution of strong shocks. The typical shock width is two or three computational cells. Because the Riemann solver used in CAVEAT is noniterative, the computational effort is roughly equivalent to that required for an artificial viscosity calculation.

The following calculations were done using CAVEAT, a three-dimensional ALE (arbitrary Lagrangian/Eulerian) computer code that solves the Euler equations of motion for a compressible fluid. The code contains a rezoning algorithm that can be invoked to translate the mesh points at the end of a time step, thus maintaining even spacing throughout the mesh. Through the option of continuous rezoning (rezoning after each time step) the code can be run in an Eulerian or Lagrangian mode. A third option exists that can be called "rezoned Lagrangian" and involves specifying Lagrangian surfaces. As a Lagrangian surface deforms, points lying on the surface remain on the surface but can be rezoned with respect to one another. CAVEAT is thus well-suited to solving problems involving severe distortions, that is, problems in which Lagrange points that are initially evenly spaced are later spaced in a highly irregular way.

The original two-dimensional version of CAVEAT was developed by the T-3 group at Los Alamos National Laboratory in 1985 [2]. J. R. Baumgardner of LANL subsequently wrote a 3D version that was both faster and more storage-efficient, although it lacked many of the features of the original code. A new 2D version that is several times faster than its predecessor was adapted from this 3D code, and some missing features were restored. The code used in the following calculations is a version of Baumgardner's 3D CAVEAT to which some additional features have been added, including the capability of running in a purely Lagrangian mode and of specifying the velocity on the boundary of a mesh. Differences in the versions of the code will be mentioned occasionally herein.

The following report consists of three sections. Section 1 contains an overview of some of the major features of the code. A derivation of the approximate Riemann solver is given in Section 2, and in Section 3 we present results obtained for the chosen test problems. Most of these results were obtained by running the code in a purely Lagrangian mode. As an Eulerian code the method is somewhat more diffusive, as might be expected. Since the remapping phase of the algorithm currently

uses a simple noniterative rezoner which produces an evenly spaced mesh, a continuously rezoned Lagrangian calculation is equivalent to an Eulerian calculation if the initial mesh spacing is regular and the boundaries are stationary. Thus the error induced in a Lagrangian calculation as a result of rezoning is of the same type as is seen in an Eulerian calculation, although it is not as severe if the boundaries are moving Lagrange surfaces.

Two of the test problems discussed in Section 3 would lose their significance if rezoning were employed. The first of these is the Saltzman problem, which consists of a piston moving into a cylinder containing a uniform gas. The difficulty lies in the configuration of the two-dimensional mesh, in which the vertical lines are not parallel to the piston and, hence, are not parallel to the shock that results from the motion of the piston. This problem is examined in more detail in the paper by Saltzman and Colella [4], in which they present a second-order Lagrangian Godunov solution obtained using an unsplit, corner-coupled algorithm. A similar piston problem is the Leblanc problem, a one-dimensional problem in which the mesh spacing in the direction of the motion of the piston (and shock) is uneven. In both of these cases rezoning would, after the first time step, transform the problem to a simpler one with an evenly spaced rectangular mesh. We hasten to add that this capability is beneficial under most circumstances, and it is only for the purpose of demonstrating the effectiveness of the Godunov method that we dispense with rezoning.

1. Features of the Code

All primary variables in CAVEAT such as velocity, pressure, density, and total and internal energies are stored at the centers of the computational cells. In the second-order calculation gradients are stored as well, and variables are assumed to be distributed linearly throughout the cell. This provides natural initial conditions for a Riemann problem at each cell face. Each cell consists of a single material, and material interfaces are assumed to coincide with cell faces. In the rezoned Lagrangian mode, material interfaces are treated as Lagrange surfaces, and interiors are rezoned to accommodate distortion of the boundaries. The velocities of vertices on Lagrange surfaces are calculated from the 12 surrounding face velocities using a least squares method. Face velocities are those provided by solution of the Riemann problem. Running in a purely Lagrangian mode requires calculation of the Lagrangian velocities of vertices in the interior of the mesh as well, and this is again done by a least squares method using the 12 surrounding face velocities.

Although the mesh generator in CAVEAT can create spherical, cylindrical, or rectangular blocks of mesh, the locations of vertices are described in terms of x, y, and z coordinates, and cell-centered vector quantities have x, y, and z components. All cells are thus arbitrary hexahedra, and cells surrounding the origin of a sphere or lying along the axis of a sphere or cylinder have degenerate faces, i.e., faces with

zero area. The logically rectangular structure of the mesh is maintained throughout the calculation, and the initial connectivity of the mesh is maintained, so that the "nearest neighbors" of a vertex point do not change.

CAVEAT solves three one-dimensional Riemann problems corresponding to the three logical mesh directions. For each face separating two cells, a one-dimensional Riemann problem in the direction normal to the face is solved. The velocities involved in this Riemann problem are the normal (to the face) components of the two cell-centered velocities. The resulting face velocity is therefore always in the direction normal to the face. A layer of ghost cells surrounds the mesh, and inflow, outflow, reflective (free slip or zero gradient), periodic, applied pressure, specified velocity, or internal boundary conditions are enforced by filling these ghost cells with the appropriate values of the cell-centered variables. This obviates satisfaction of boundary conditions by the Riemann solver, as every cell face appears to be in the interior of the mesh. The specified velocity boundary condition is an option that has been added at LLNL and as yet does not exist in other versions of the code. This boundary condition is necessary for all piston problems.

CAVEAT is explicit and first-order accurate in time, and first- or second-order accurate in space, as specified by the user. Flux limiting reduces the spatial accuracy to first order locally, but suppresses oscillations in the second-order solution. The user can specify monotone or Van Leer limiting. Monotone limiting may be preferable for cases when Van Leer limiting results in unwanted oscillations; however, although some of the results presented in Section 3 do exhibit small oscillations, we have not found an example in which the oscillations were severe enough to warrant use of the more diffusive monotone limiting. Because the Riemann solver used in CAVEAT is noniterative, the computational effort is roughly equivalent to that required for an artificial viscosity calculation. The cost of a second-order solution is greater by a factor of three than the cost of a first-order solution, and a second-order solution increases the memory requirements. Thus the user may, particularly for problems for which the solution is expected to be smooth, choose to do a first-order calculation. In Section 3, we compare first- and second-order solutions for several of the test problems.

2. The Algorithm

The algorithm employed in CAVEAT breaks down into three steps: a Lagrangian solution of the momentum and work equations, a rezone step in which vertex velocities are chosen using a simple one-step noniterative rezoner, and a conservative advection step in which quantities are remapped onto the new mesh. In this section, we present a brief discussion of the first of these three steps. A more complete derivation of the approximate Riemann solver used in CAVEAT can be found in Ref. [1].

The Godunov method solves the Lagrangian form of the momentum and work equations:

$$m_k \frac{d\bar{\mathbf{u}}_k}{dt} = -\int_{S_k} p\mathbf{n}\, dA \tag{2.1}$$

and

$$m_k \frac{d\bar{E}_k}{dt} = -\int_{S_k} p\mathbf{u}\cdot\mathbf{n}\, dA. \tag{2.2}$$

Here m_k is the cell mass, given by

$$m_k = \int_{V_k} \rho\, dv,$$

the cell-averaged velocity is given by

$$\bar{\mathbf{u}}_k = \left(\frac{1}{m_k}\right)\int_{V_k} \rho\mathbf{u}\, dv,$$

and

$$\bar{E}_k = \left(\frac{1}{m_k}\right)\int_{V_k} \rho\left(e + \frac{1}{2}\mathbf{u}\cdot\mathbf{u}\right) dv$$

is the cell-averaged total energy. In addition, p is the pressure, ρ is the density, e is the specific internal energy, $\mathbf{u}$ is the velocity, V_k is a control volume, taken to be the kth cell in the calculations, and S_k is its surface. The unit vector normal to S_k is $\mathbf{n}$. The pressure is assumed to be of the form

$$p = p(\rho, e). \tag{2.3}$$

To advance the solution of (2.1) and (2.2) in time requires knowledge of the pressure and velocity on cell faces. To obtain these values, each pair of cells is treated as a Riemann problem, with initial conditions given by the cell-centered values of ρ, e, p, and u on either side of the face, where u is the component of the cell-centered velocity that is normal to the face. Thus, at the beginning of each time step, the cell face represents a discontinuity in some or all of these quantities. This discontinuity induces a shock, a rarefaction, and a contact discontinuity across which the density and internal energy may differ but the pressure and velocity are the same. Schematically, this can be represented by an x-t diagram, as is shown in Fig. 1. Lines A and B represent a pair of waves consisting of a shock and a rarefaction traveling outward from the original discontinuity, and line C is the contact discontinuity, across which p^* and u^* do not change. CAVEAT uses an approximate Riemann solver to find the values of p^* and u^*, after which the surface integrals in Eqs. (2.1) and (2.2) can be evaluated by summing over cell faces.

One of the advantages of using a Riemann solver instead of artificial viscosity lies in the fact that solution of the Riemann problem requires no explicitly user-

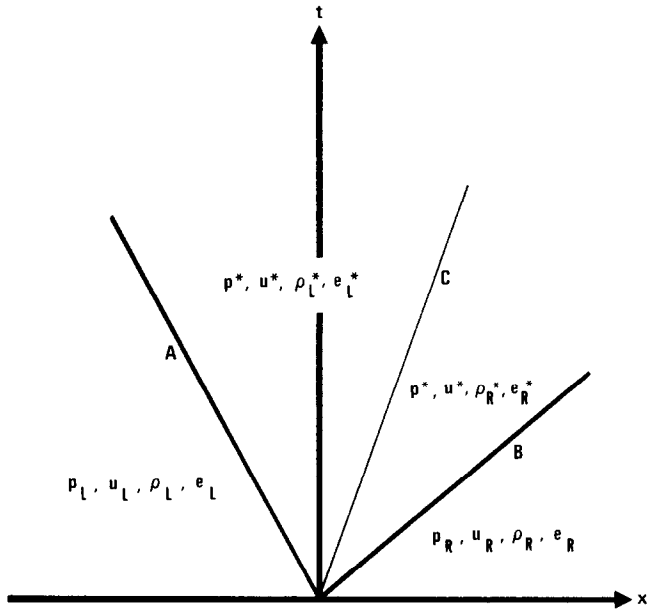

FIG. 1. The system of waves representing the solution to the Riemann problem.

specified parameters. Such parameters occur in the use of an artificial viscosity when one is forced to decide on values for coefficients of the linear and quadratic terms in an expression for q. The Riemann solver described herein instead contains two material-dependent parameters, which will be examined in greater detail below.

We will use the notation q_+, q_- to denote a quantity in front of and behind a shock, respectively, and the difference across the shock will be denoted by δq. By rewriting the Rankine–Hugoniot relations, and by assuming that $p = p(e, \rho)$, we can express δp as

$$\delta p = \pm |f(\delta p, \delta u)|\, \delta u, \tag{2.4}$$

for a shock, and

$$\delta p = \pm |g(\delta p, \delta u)|\, \delta u, \tag{2.5}$$

for a rarefaction. The choice between signs is made according to the direction of the shock or rarefaction. The choice between the two equations (shock or rarefaction) is made according to the sign of $p_+ - p_-$; e.g., a shock to the right is described by $\delta p = |f|\, \delta u$, while $\delta p = -|g|\, \delta u$ describes a rarefaction to the left. For materials such as an ideal gas these two equations can be solved simultaneously for the pressure and velocity of the contact discontinuity between a shock and a rarefaction. However, for all but the simplest equations of state, it is difficult if not

impossible to find expressions for f and g. Two simplifying assumptions will thus be made.

The two-shock approximation was first used in a Riemann solver by Colella [5]. By examining the Rankine–Hugoniot equations one can infer that

$$|g| = |f| + O\left(\delta \frac{1}{\rho^2}\right). \tag{2.6}$$

Thus for relatively weak waves, the shock-Hugoniot (the p versus ρ curve that results when the velocity is eliminated from the Rankine-Hugoniot relations) is a good approximation to the rarefaction-Hugoniot. Furthermore, rarefactions can be expected to be weak (no steep gradients) even when the corresponding shocks are strong. Therefore, we will assume that the system consists of two shocks and a contact discontinuity.

The next step is to find an approximate form for the shock-Hugoniot. Consider the use of artificial viscosity, in which the cell pressure used in the momentum and energy equations is given by

$$p' = p + q, \tag{2.7}$$

where p is the usual pressure and q is a function of the velocity gradient. One commonly used form for q, which has the effect of a bulk viscosity, is a combination of the Von Neumann quadratic form [6] and a linear form suggested by Landshoff [7]:

$$q = C_0^2 \rho\, \Delta u^2 + C_L \rho a_0 |\Delta u|. \tag{2.8}$$

There is some uncertainty in the choice of the coefficients, but the usual choices are $C_0 \approx 2$ and $C_L \approx 1$.

For two cases in which the equation of state is simple enough to find an expression for $|f|$ (an ideal gas and an elastic solid), the resulting expressions for $\delta\rho$ are very similar to the quadratic and linear forms used for q, for strong and weak shocks, respectively. This similarity has been used occasionally to find values for the artificial viscosity coefficients C_0 and C_L. Reversing this process, assume that the shock-Hugoniot takes the form

$$C_0^2 \rho\, \delta u^2 + C_L \rho a_0 |\delta u|, \tag{2.9}$$

where a_0 is the local sound speed, and use

$$|f| = \rho(a + A\,|\delta u|) \tag{2.10}$$

for $|f|$, where a is obtained from the weak shock limit and A from the strong shock limit.

From the Rankine–Hugoniot relations, we can deduce that

$$a = a_0, \qquad \text{the local sound speed,}$$

and

$$A = \lim_{|\delta u|/a_0 \to \infty} \left\{ \frac{(\rho_-/\rho_+)}{(\rho_-/\rho_+) - 1} \right\}. \tag{2.11}$$

For an ideal gas,

$$\frac{\rho_-}{\rho_+} = \frac{\gamma + 1}{\gamma - 1}$$

in the strong shock limit, so $A = (\gamma + 1)/2$. Here γ has the same value as in the ideal gas equation of state $p = (\gamma - 1)\,\rho e$. This approximation to the shock Hugoniot is excellent for a variety of materials. Comparisons with experimental Hugoniot data and further justification of the approximation can be found in Ref. [1].

For rightward propagating waves, we now have

$$p_L - p_R = \rho_R(a + A(u_L - u_R))(u_L - u_R) \tag{2.12}$$

and this is the equation for either a shock or a rarefaction. If the wave is a rarefaction, then this expression is only valid for $\delta u \geqslant -a/2A$, and so we rewrite this as

$$p_L - p_R^* = \rho_R A\, |u_L - u_{\min}^*|\, (u_L - u_{\min}^*), \tag{2.13}$$

where

$$p_R^* = p_R - \frac{1}{4}\rho_R \frac{a^2}{A}$$

and

$$u_{\min}^* = u_R - \frac{a}{2A}.$$

For leftward propagating waves, the analogous equation is

$$p_R - p_L^* = -\rho_L A\, |u_R - u_{\max}^*|\, (u_R - u_{\max}^*), \tag{2.14}$$

where

$$p_L^* = p_L - \frac{1}{4}\rho_L \frac{a^2}{A}$$

and

$$u_{\max}^* = u_L + \frac{a}{2A}.$$

If these two equations represent the solution to a Riemann problem, then

$$p_L = p_R = p^*,$$
$$u_L = u_R = u^*,$$

and these are the pressure and velocity of the contact discontinuity. These equations can be rewritten, since

$$p^* - p_R^* = \rho_R A \, |u^* - u_{\min}^*| \, (u^* - u_{\min}^*), \tag{2.15}$$

and

$$p^* - p_L^* = -\rho_L A \, |u^* - u_{\max}^*| \, (u^* - u_{\max}^*). \tag{2.16}$$

Equations (2.15) and (2.16) can now be solved simultaneously for u^* and p^*. By considering cases and assuming signs for $|u^* - u_{\min}^*|$ and $|u^* - u_{\max}^*|$, elimination of p^* results in a quadratic equation for u^*. This can be solved in the usual straightforward way, and back substitution of u^* can then be used to find p^*. Cavitation is predicted when $p^* < 0$, in which case p^* can be set equal to 0, and the two equations for u^* can be solved for the velocities of the two resulting faces.

3. Test Problems

The first test problem chosen was a Noh problem (implosion) on a regular rectangular mesh. This is a one-dimensional problem in which a confined volume of gas has initial density one and zero internal energy. Since CAVEAT is a 3D code, the problem is run on a 100 by 1 by 1 mesh, and the boundaries corresponding to y and z equal to zero and one are reflective (zero-gradient). The initial velocity is minus one in the interior and on the right, and a reflective boundary condition is applied on the left. As the gas becomes compressed at this wall, a shock forms at the left boundary and moves from left to right. Using a γ-law equation of state with γ equal to $\frac{5}{3}$, the correct density profile is given by $\rho = 4$ behind the shock and $\rho = 1$ in front of the shock. A complete discussion of this problem in rectangular, cylindrical, and spherical geometries can be found in the report by Noh [8].

The density plots shown in Figs. 2 and 3 were made at approximately $t = 0.6$, when the right wall has reached $x = 0.4$ and the shock has reached $x = 0.2$. In Fig. 2, first-order solutions with and without rezoning are compared, and in Fig. 3, a second-order solution without rezoning is shown. As would be expected, the rezoned solution is more diffusive than the first-order solution without rezoning, which is smoother than the second-order solution. The second-order solution, while exhibiting greater error at the wall, contains an extremely well-resolved shock. This error at the wall, which is generally referred to as wall-heating or wall-cooling (depending on the sign of the error in the specific internal energy), appears in most solutions to problems involving a non-physical impulsive start. This is true of not

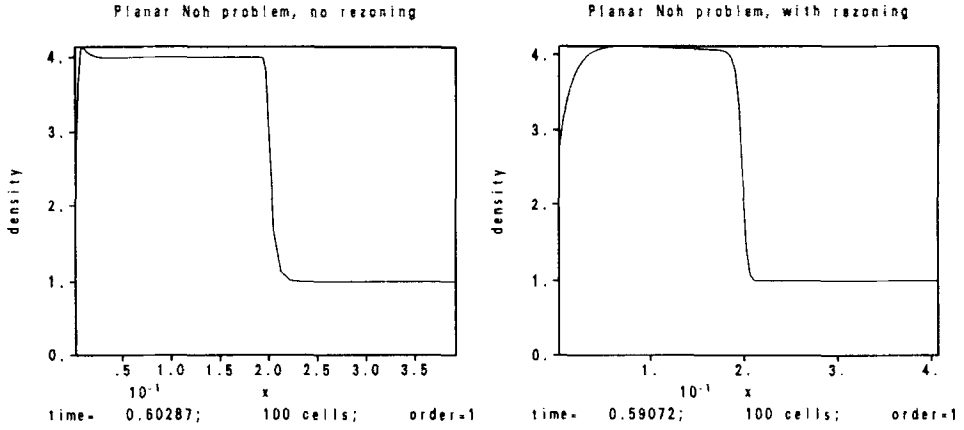

FIG. 2. The Noh problem on a regular rectangular mesh; first-order solutions with and without rezoning.

only Godunov solutions but other Lagrangian solutions as well. A discussion of this effect, which occurs at the location of the formation of the shock, can be found in the paper by Noh [9]. In this paper, Noh suggests an "artificial heating" correction to reduce the error; however, this correction does not affect the error throughout the rest of the domain. For this reason, we have chosen to ignore the problem of wall-heating.

A density profile and initial and final mesh plots are shown (Figs. 4 and 5) for the same problem on a cylindrical mesh. Now the exact solution is given by $\rho = 16$ for $r < 0.2$ (behind the shock), $\rho = 4$ for $r = 0.2+$ (in front of the shock), and $\rho = 1 + t/r$ for $0.2 < r < 0.4$. The broken line in Fig. 4 is $\rho = 16$, and it can be seen that this first-order solution without rezoning has a relative error of about 4% behind the shock.

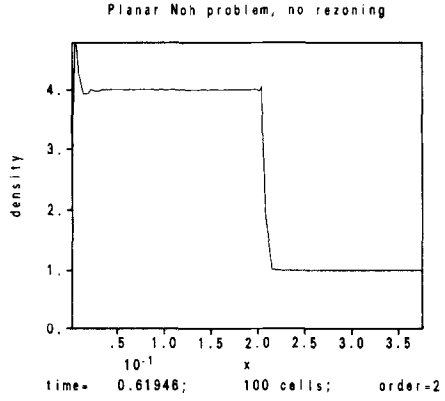

FIG. 3. The Noh problem on a regular rectangular mesh; second-order solution without rezoning.

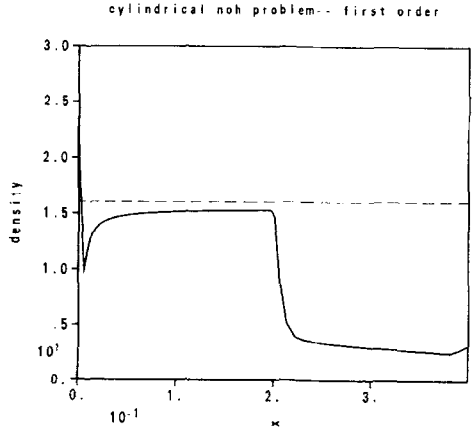

FIG. 4. The Noh problem on a cylindrical mesh; first-order solution without rezoning.

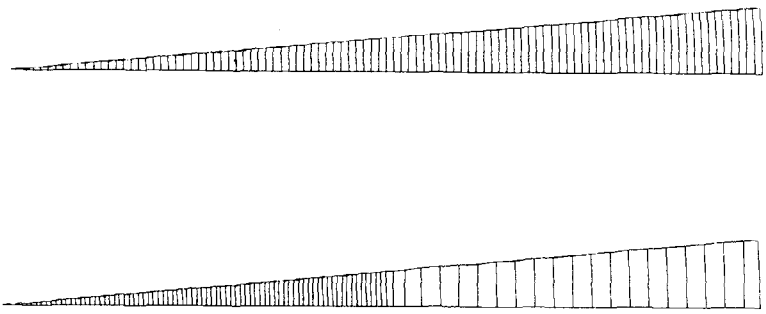

FIG. 5. Initial and final mesh plots for the cylindrical Noh problem.

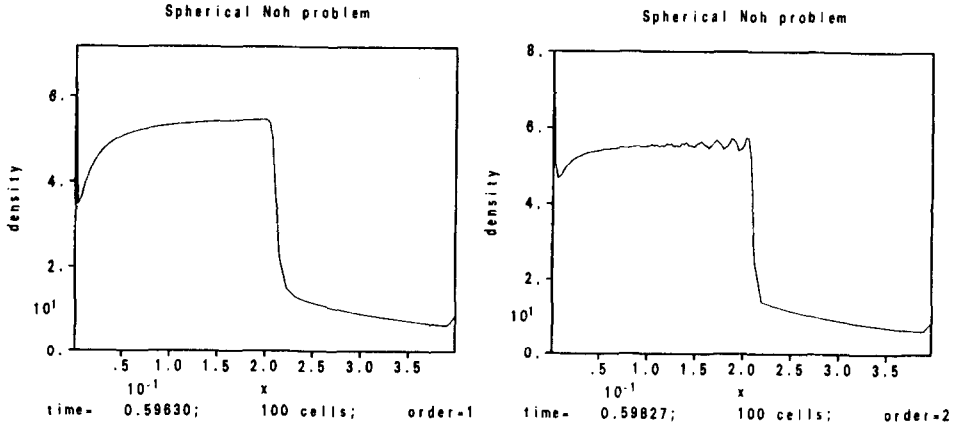

FIG. 6. The Noh problem on a spherical mesh; first- and second-order solutions without rezoning.

FIG. 7. Spherical Noh problem; mesh configuration at $t = 0.6$.

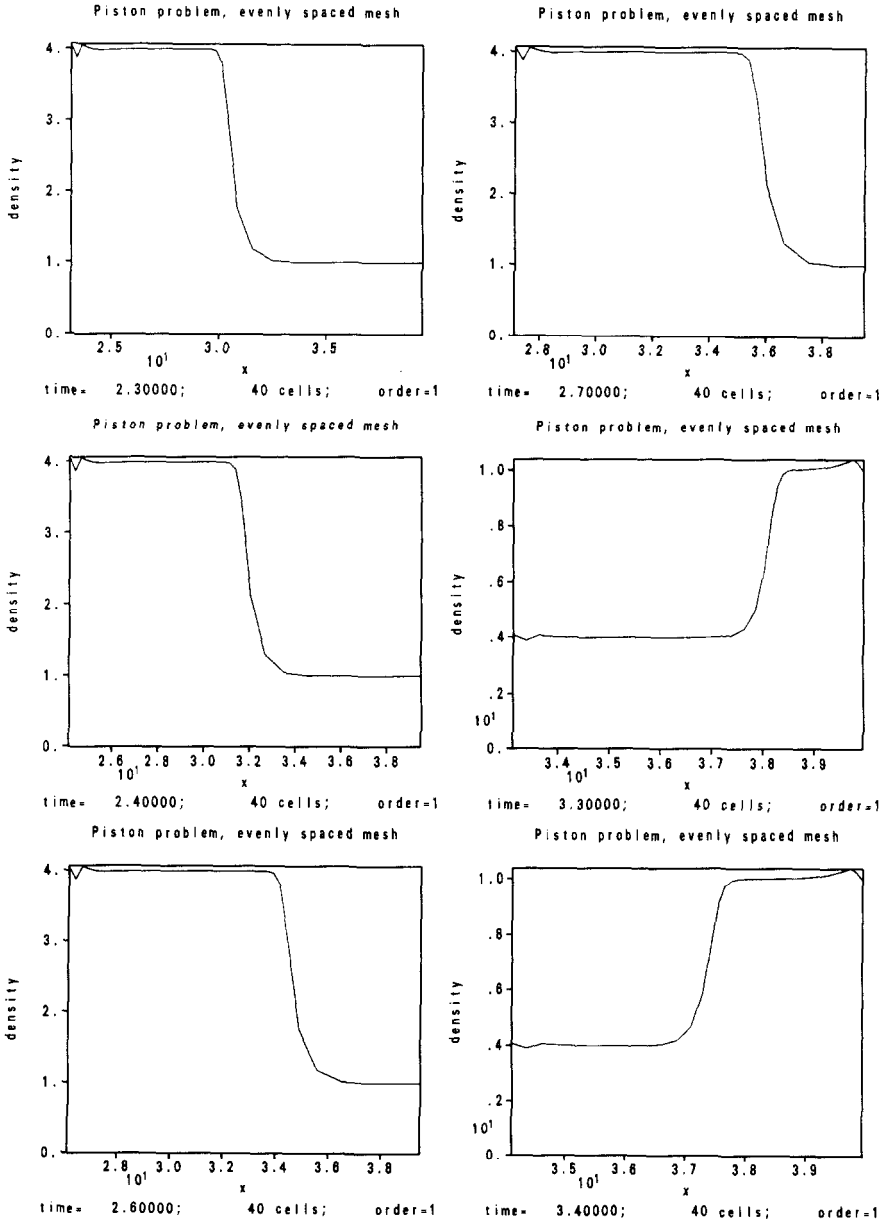

FIG. 8. First-order solution of the piston problem on an evenly spaced forty-zone mesh; a time-history of the density.

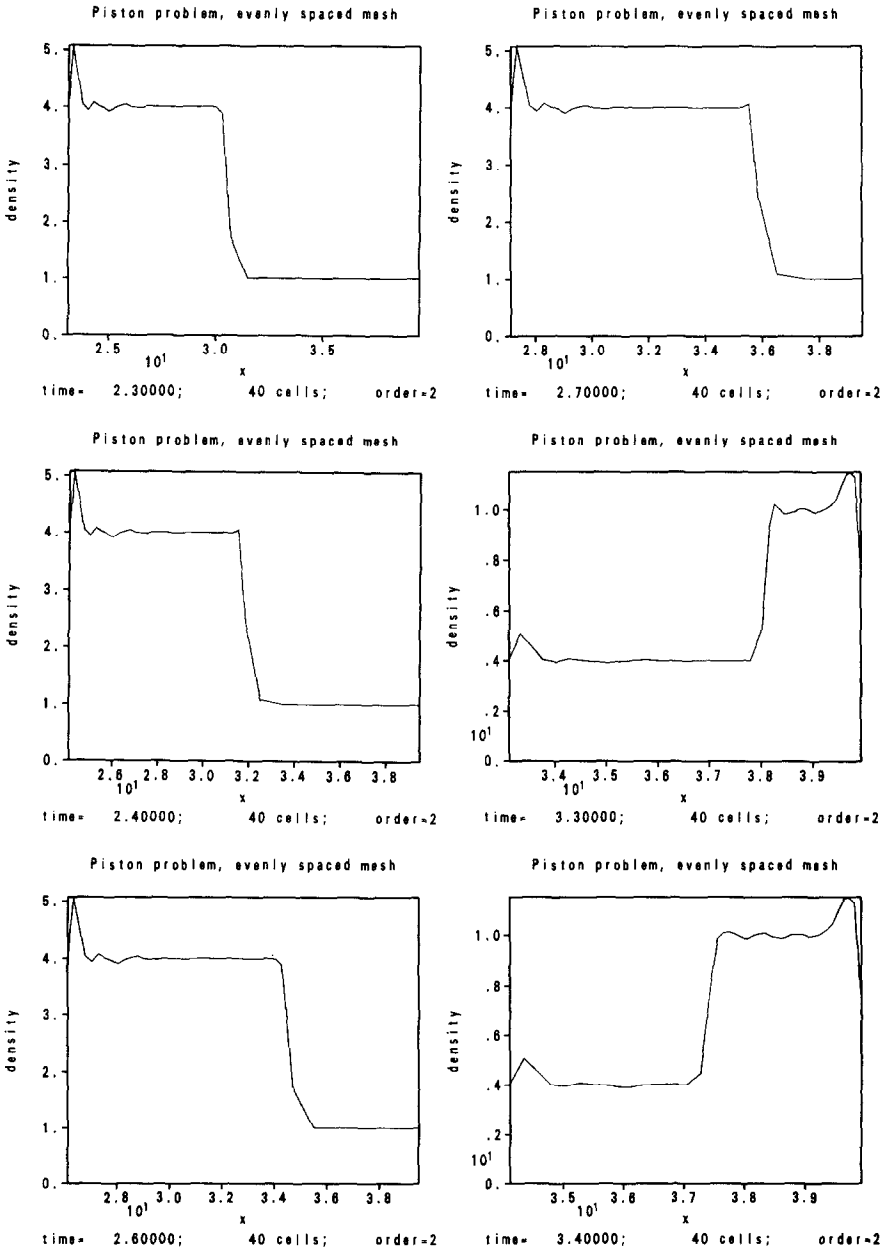

FIG. 9. Second-order solution of the piston problem on an evenly spaced forty-zone mesh; a time-history of the density.

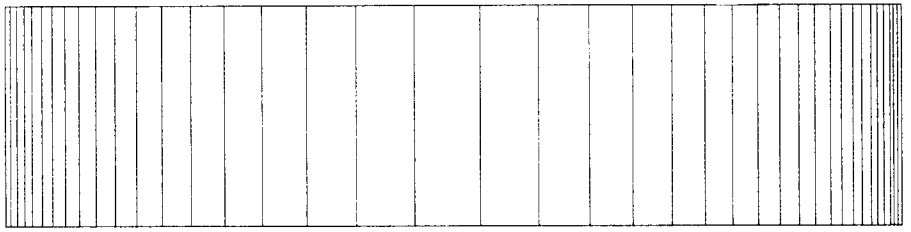

FIG. 10. Initial mesh configuration for the Le Blanc piston problem.

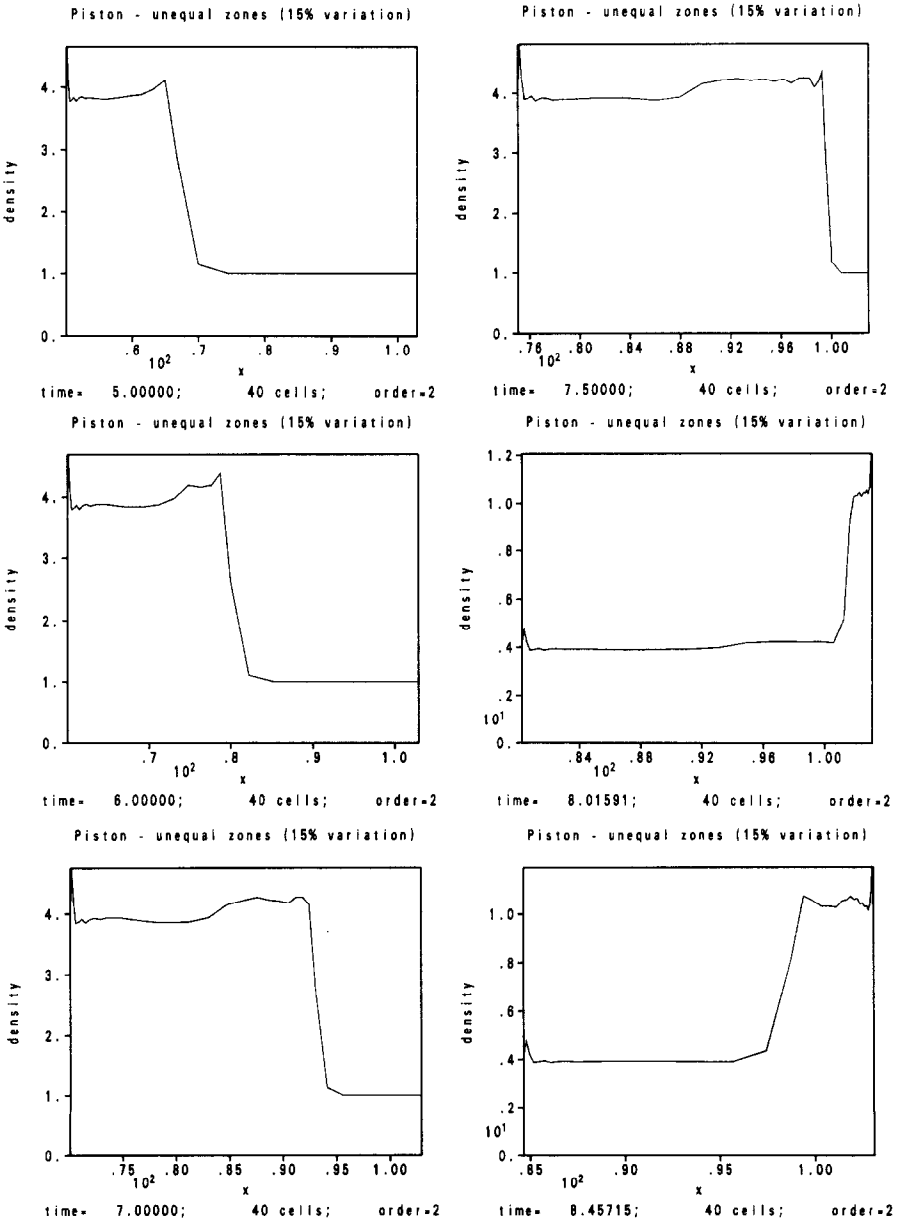

FIG. 11. Second-order solution of the Le Blanc problem; a time-history of the density.

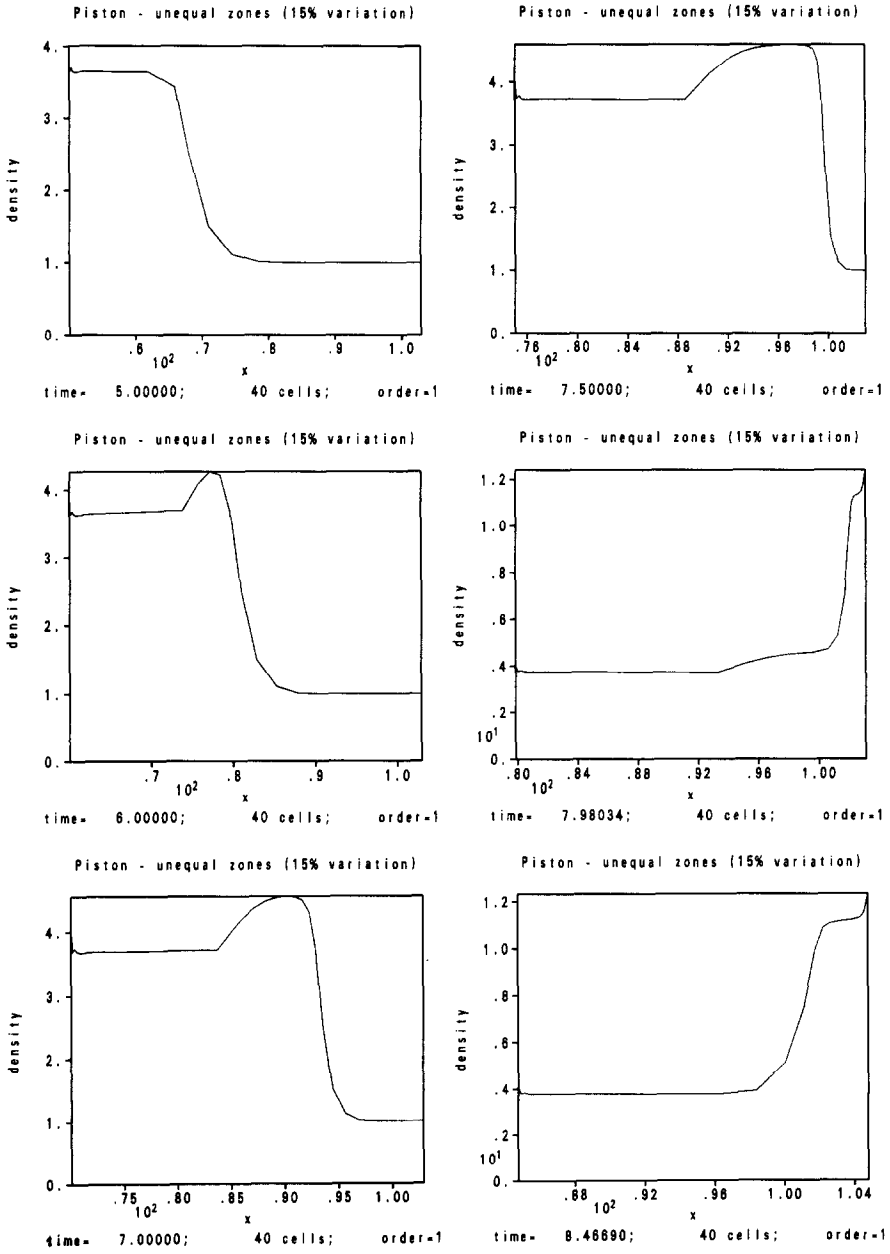

FIG. 12. First-order solution of the Le Blanc problem.

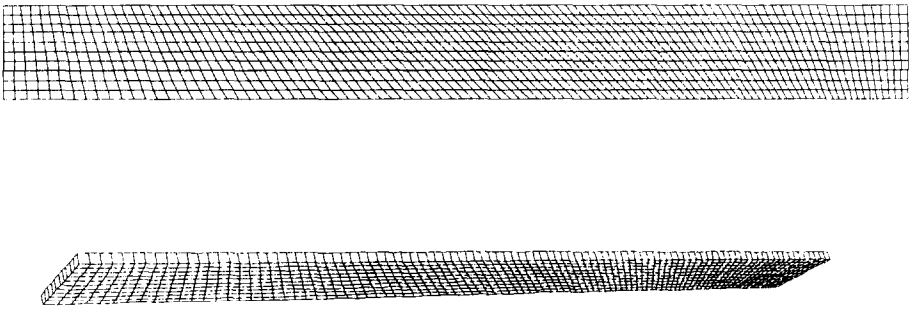

FIG. 13. Initial mesh configuration for the Saltzman piston problem.

Figures 6 and 7 show the same information for the Noh problem on a spherical mesh. The exact value of the density behind the shock is now 64, which is indicated by the broken lines in both of the plots in Fig. 6. Here both first- and second-order solutions were obtained, with the result that the first-order solution, while being smoother, has both a greater error at the left wall and a greater error just behind the shock. Problems with the dimensions of cells surrounding the origin prevent fine enough zoning to produce a more accurate result to this problem. A more sophisticated mesh generator is being developed that will, we hope, improve the quality of the solution.

The next three test problems are piston problems, and differ only in the mesh used. In each of these problems, a cylinder is filled with a uniform γ-law gas that is initially at rest. As a piston moves in from the left, a shock forms and moves out ahead of it. In each of these three problems, the correct value of the density behind the shock is four, and the undisturbed gas in front of the shock has a density of one. Figures 8 and 9 contain time-histories of the densities for an evenly spaced mesh with 40 zones. The solution is first-order in Fig. 8 and second-order in Fig. 9. Rezoning is not done in these or any of the piston calculations. In the first frame in Fig. 8, the piston has moved in to $x = 23$, and the shock has moved approximately three quarters of the way down the cylinder. The shock hits the right

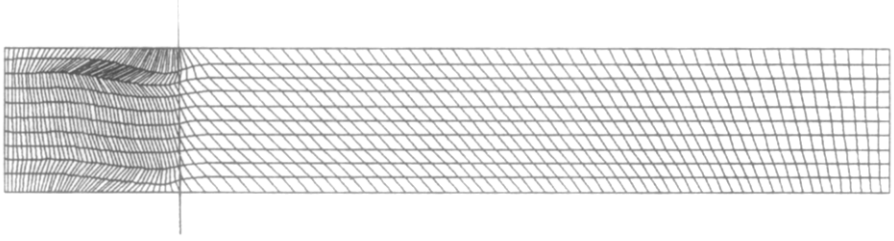

FIG. 14. The Saltzman mesh at $t = 0.375$. The vertical line indicates the location of the shock at $x = 50$, halfway across the original mesh.

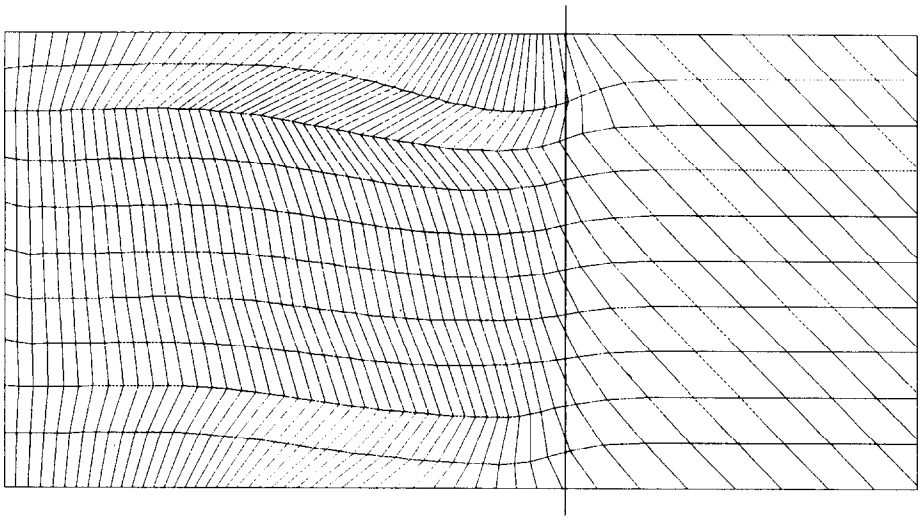

FIG. 15. A closeup of the Saltzman mesh behind the shock at $t = 0.375$. The vertical line indicates the location of the shock at $x = 50$.

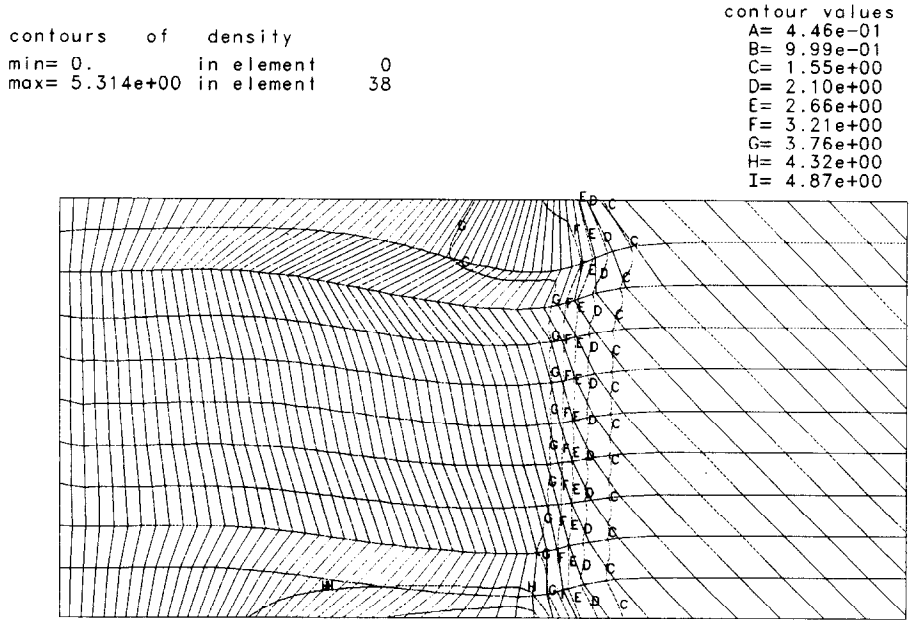

FIG. 16. Density contours superimposed on Fig. 15.

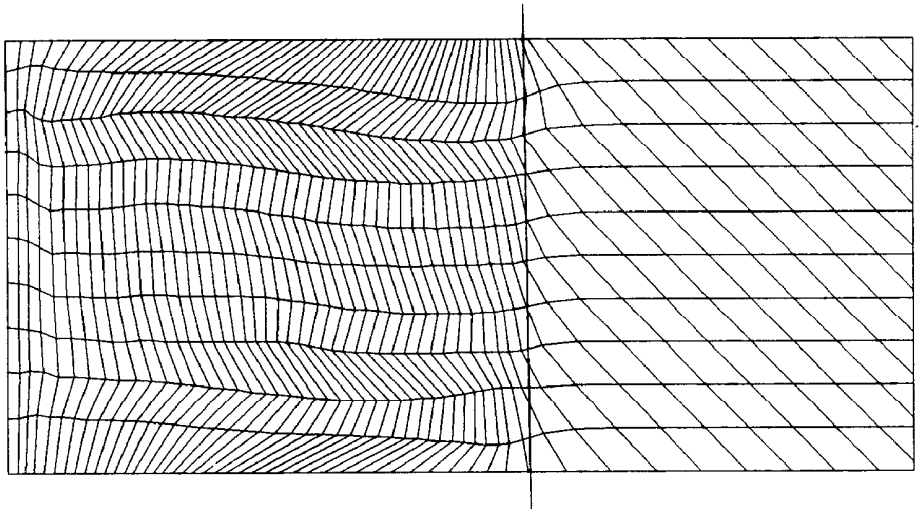

FIG. 17. The mesh behind the shock resulting from the second-order solution of the Saltzman problem. As in Fig. 15, $t = 0.375$.

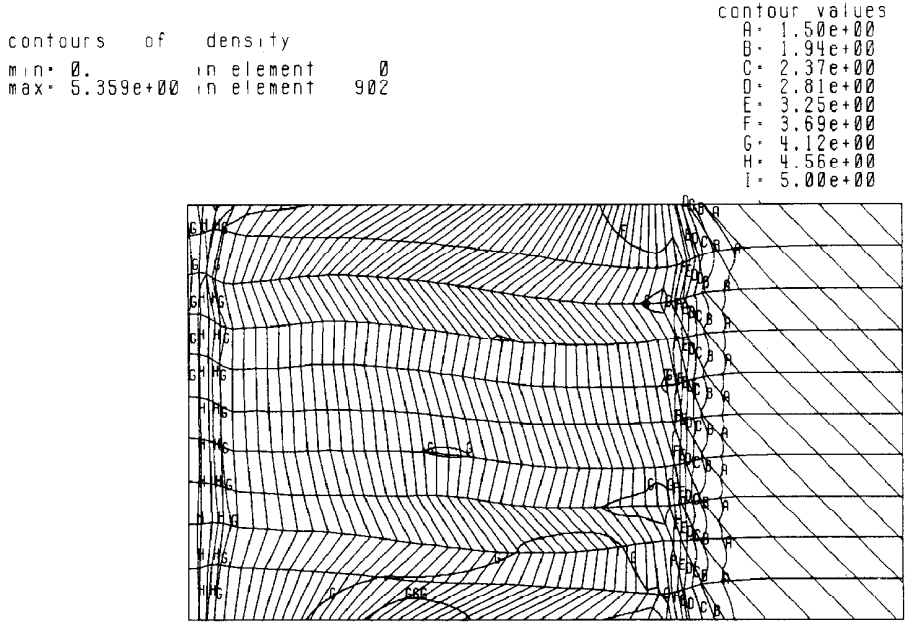

FIG. 18. Density contours superimposed on Fig. 17.

FIG. 19. The actual configuration of the Saltzman mesh with large aspect ratio cells at $t = 0.5$.

wall at $t = 3$ (not shown) and is reflected. As can be seen by comparing Fig. 8a with Fig. 2a, the accuracy of the results is consistent with that obtained for the rectangular Noh problem. These two problems are physically equivalent, differing only in the location of the stationary frame of reference. Again, the greatest error occurs at the location at which the shock first forms, this time at the moving wall.

Figure 10 shows the initial mesh configuration used next. As in the previous case, there are 40 cells in the horizontal (x) direction, but now the cell widths increase by 15% in the left half of the mesh ($dx(n+1) = 1.15dx(n)$ for $n < 20$) and decrease by 15% in the right half. This problem, sometimes called the Le Blanc problem, is also discussed in Ref. [9], although most of the results presented therein are for a less severely varying mesh having a 5% gradient in cell widths rather than 15%. In contrast to the previous problem, in which the first-order solution on the evenly

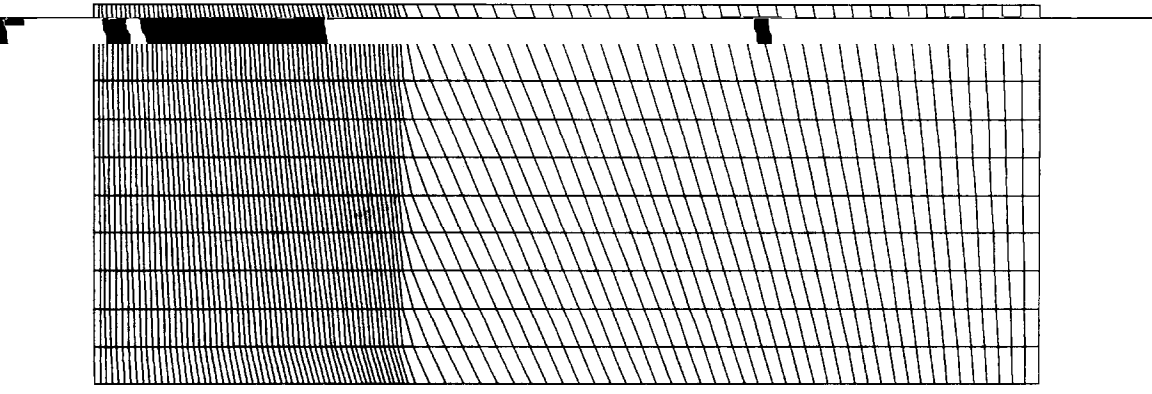

FIG. 20. The mesh in Fig. 19 has been scaled using a post-processor; $t = 0.5$.

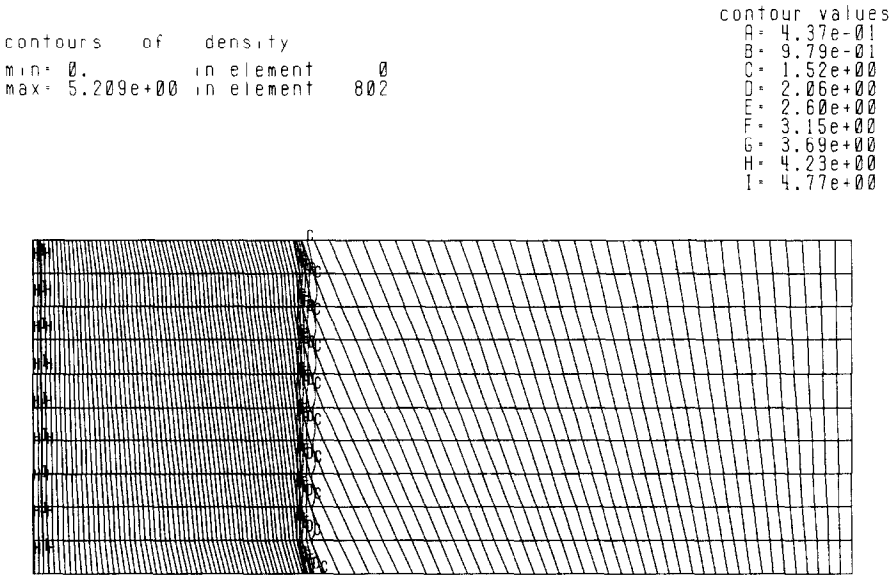

FIG. 21. Density contours superimposed on Fig. 20.

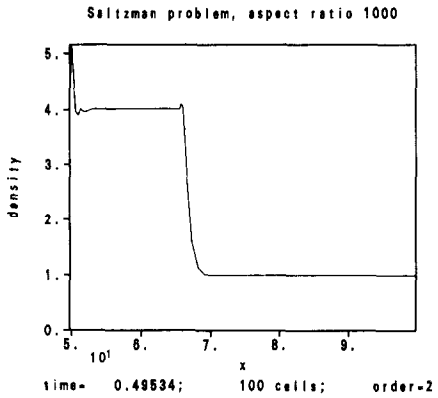

FIG. 22. The density profile corresponding to the contours shown in Fig. 21.

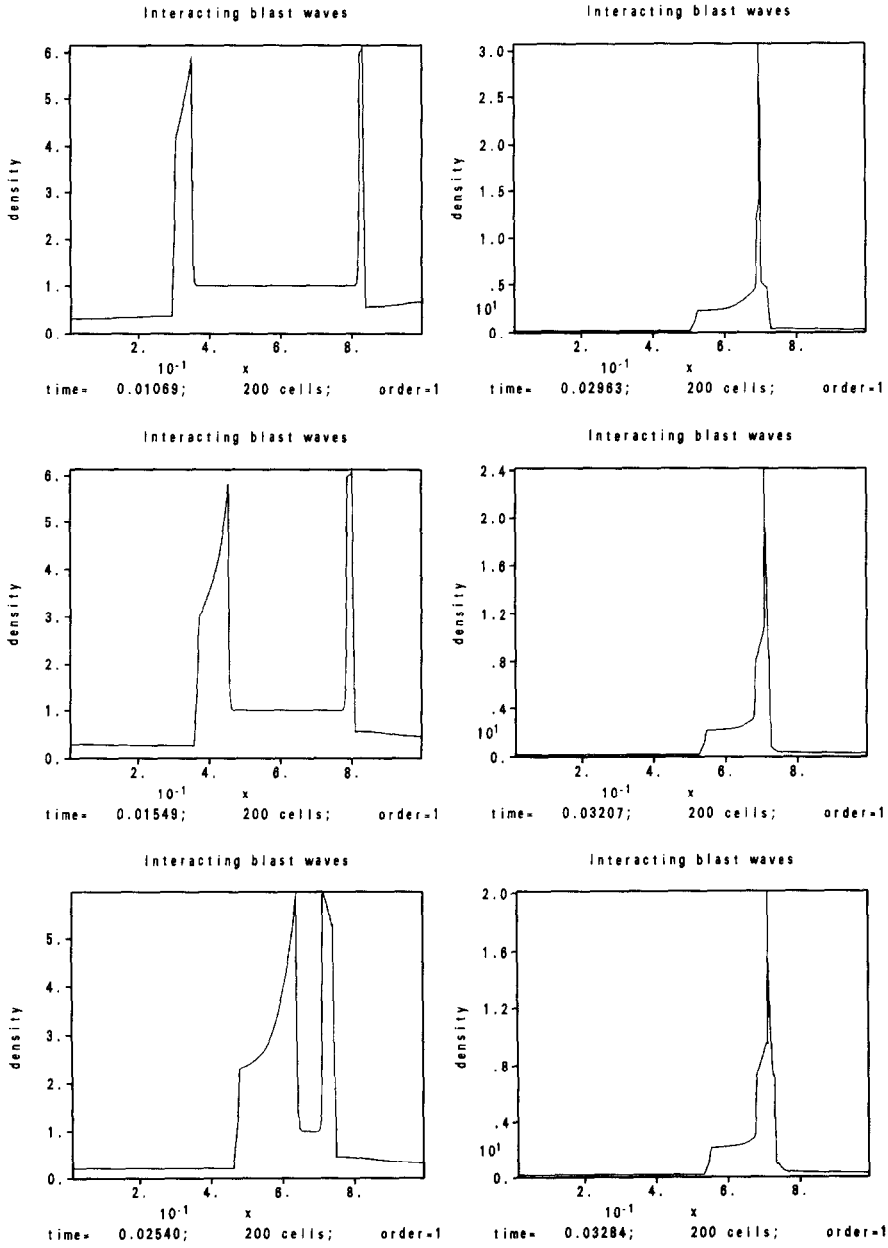

FIG. 23. A time-history of the density profile for interacting blast waves; first-order solution.

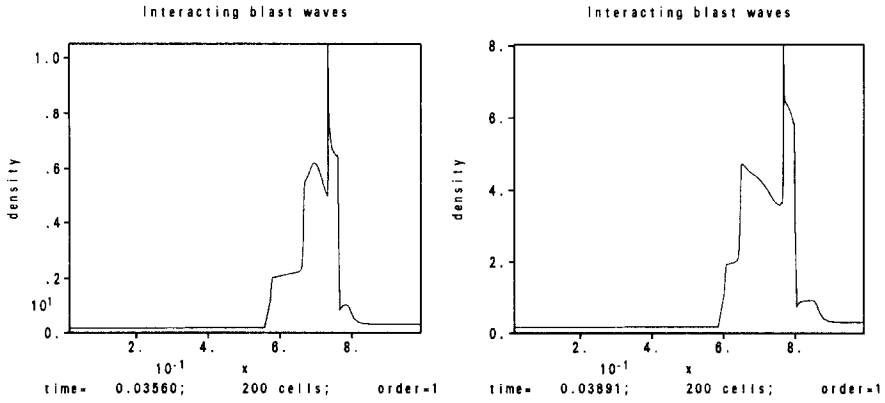

FIG. 23—*Continued*

spaced mesh was more aesthetically pleasing due to small oscillations in the second-order solution, it is evident in this case that the second-order solution shown in Fig. 11, having a relative error of approximately 7% behind the shock, is preferable to the first-order solution shown in Fig. 12. The first-order solution is, however, considerably more accurate than that presented in Ref. [9], in which the error in the density behind the initial shock is as great as 40%.

Among the three piston problems discussed in this report, the most difficult is undoubtedly the Saltzman problem [4]. Unlike the two preceding cases, the Saltzman problem is made two-dimensional by the configuration of the mesh, which is shown in Fig. 13. In the lower diagram, the figure has been rotated around the x-axis to show the actual 100 by 10 by 1 mesh. The initial length of the cylinder is 100. At time 0.375, the piston (the left wall) has moved in to $x = 37.5$, and the shock has traveled from $x = 0.$ to $x = 50.$, across half the length of the original cylinder (Fig. 14). A blowup of the portion of the mesh behind the shock is shown in Figs. 15 and 16, and density contours are superimposed on the mesh in Fig. 16. Figures 17 and 18 illustrate the second-order solution with Van Leer limiting. The location of the shock, as is indicated in Fig. 17, is again at $x = 50$. Although other solutions to this problem have not as yet appeared in the open literature, the problem has generated considerable interest at LLNL, Los Alamos National Laboratory, and elsewhere.

To test the capability of the code to handle large aspect ratio cells, the mesh was stretched in the y direction to produce cells with aspect ratio 1000. Figure 19, which resembles a thick vertical line, is actually a picture of the initial mesh after it has been compressed in the x direction and stretched in the y direction. To view the density contours resulting from running the problem on this mesh, the figures are scaled using a post-processor. The results, shown in Figures 20, 21 and 22, show that this has, in fact, improved things considerably. As can be seen in Fig. 21, the

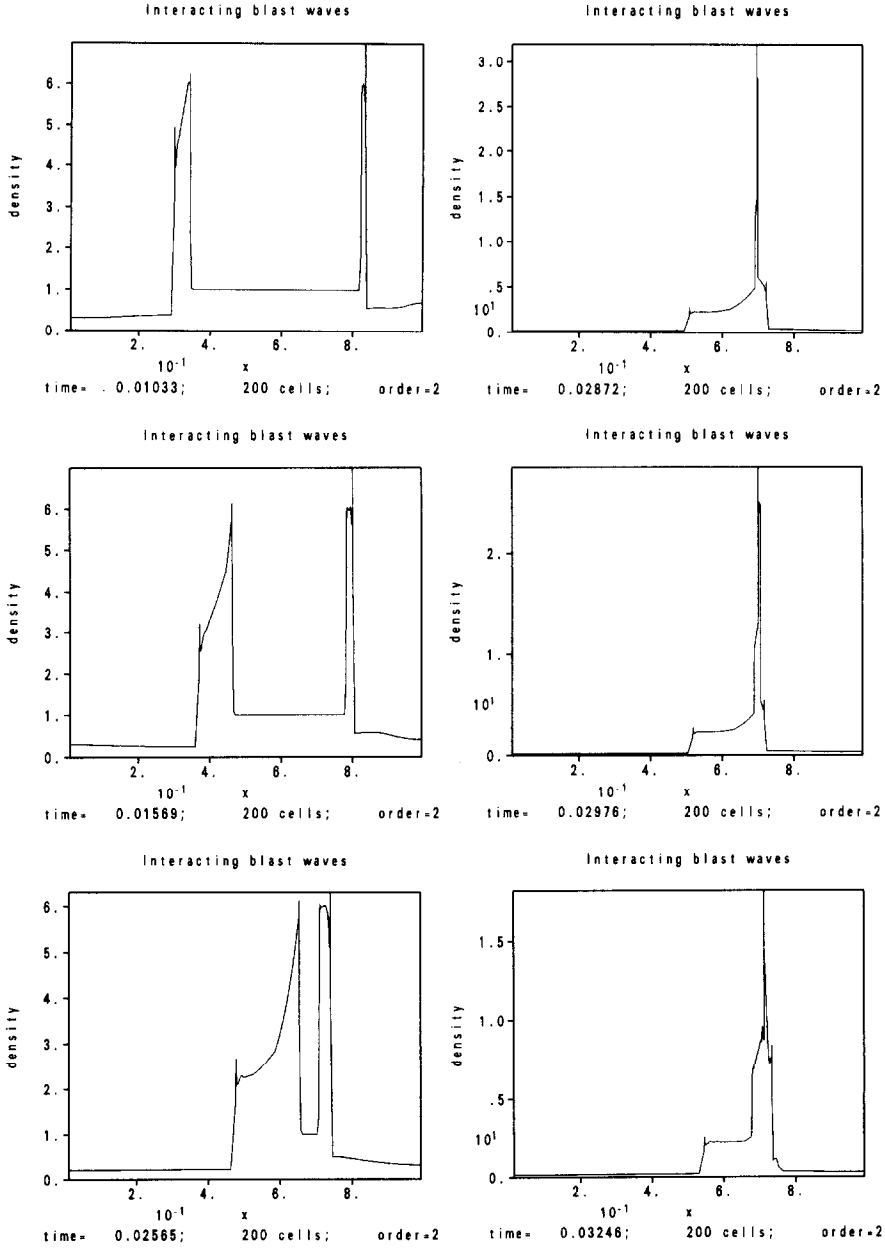

FIG. 24. A time-history of the density profile for interacting blast waves; second-order solution with Van Leer limiting.

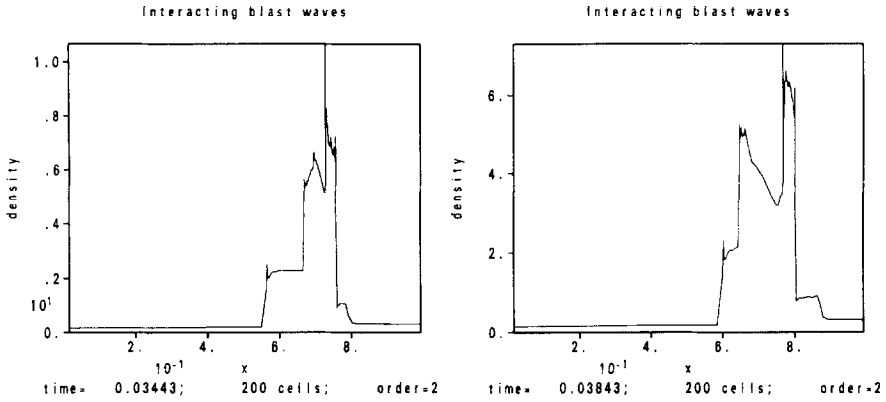

FIG. 24—*Continued*

densities are now so uniform across the width of the mesh (from the top to the bottom) that is is meaningful to examine a density profile taken along the $y = 5.$ line (Fig. 22). The companion problem in which cells have aspect ratio 0.001 is far more difficult, and satisfactory results have not been obtained by use of a Godunov method or any other method known to us.

The interaction of two blast waves is illustrated by the next set of results. The initial condition for this one-dimensional problem consists of a closed volume of γ-law gas (with γ equal to 1.4) that is of uniform density but nonuniform pressure and temperature. The pressure is initially 1000 near the left wall, 100 near the right wall, and 0.01 in the center. The specific internal energies correspond to these pressure values. The mesh consists of 200 uniform zones. The time-history of the density profile shown in Fig. 23 was obtained with a first-order calculation, and the second-order method was used to obtain the results presented in Fig. 24. The Van Leer limiting was used in this second-order calculation even though it does allow undesirable spikes to appear after the blast waves have interacted. The more diffusive monotone limiting produced results that resembled the first-order solution.

Nearly exact results for this problem were calculated in a review article by Woodward and Collela using a PPMLR scheme and treating the three regions described above as distinct fluids [9]. In their calculation, that portion of the solution preceding the interaction of the blast waves was calculated exactly. Subsequently the mesh, consisting of 3096 zones, was refined near the contact discontinuities and near the location of the collision of the two shocks. This solution was used as a benchmark, and results obtained using seven numerical methods, including a first-order Godunov scheme, were compared in their paper. Two calculations are shown for each method, one in which the mesh consisted of 200 equally spaced zones, and one in which the mesh consisted of 1200 equally spaced zones.

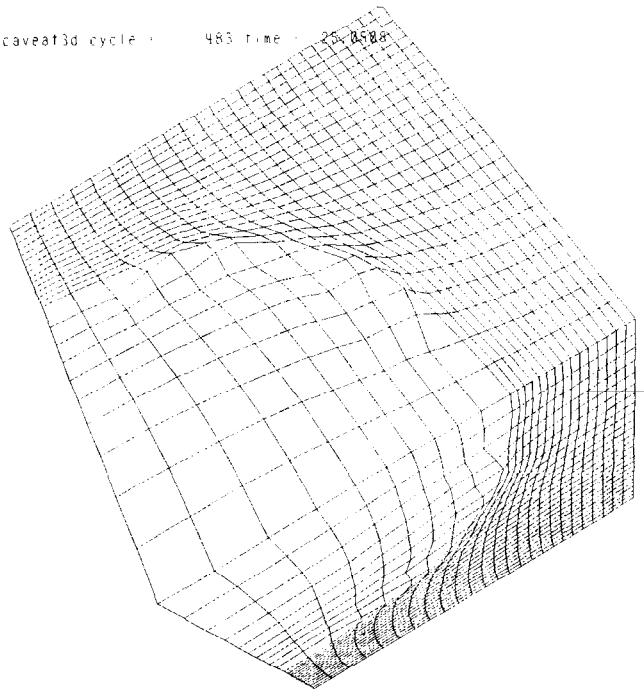

FIG. 25. A spherical expansion on a rectangular mesh.

Unfortunately it would be impractical to include all of their figures in this paper, but the results can be described qualitatively. The method described herein performed considerably better than any of the methods used in their paper on the 200-zone mesh. Only their PPMDE and PPMLR methods came close to reproducing the correct height of the peaks, sharpness of the shocks, and preservation of the structure of the solution. Their solutions, however, did not contain the spike that formed at approximately $x = 8$, or any of the spikes that appear in the second-order CAVEAT solution. Their methods all produced significantly better results when the 1200-zone mesh was used; however, CAVEAT still outperformed the first-order Godunov and MacCormack schemes.

The final test problem consists of a spherical expansion on a rectangular mesh. This problem is included only as a demonstration of the ability of the code to maintain the symmetry of the shock as it distorts the mesh. The initial mesh is a cube containing 15,625 uniform cubic cells. A 10 by 10 by 10 block of cells nearest the origin (located in a corner of the mesh) is loaded with material having a density three times that of the remainder of the mesh. This density gradient causes a shock to form and travel outward from the center. Reflective (zero gradient) boundary conditions are employed on all sides of the mesh.

In Fig. 25 the shock has progressed about three-quarters of the way across the

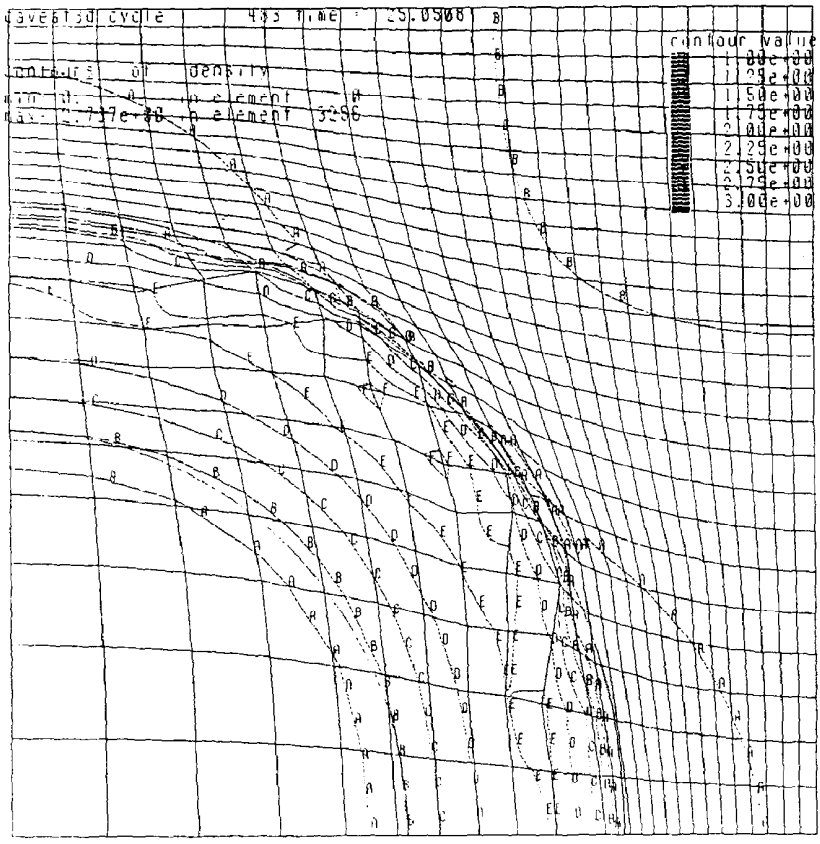

FIG. 26. Density contours superimposed on Fig. 25, rotated to show the $x - y$ plane.

mesh, and corresponding density contours are shown in Fig. 26. The symmetry of the solution is more easily ascertained from Fig. 27, in which quarter-circles centered at the origin have been drawn on the mesh. Densities are the same at all of the points indicated by dots, and thus the density contour through these points misses being spherical by less than 3%. The solution is symmetric in x, y, and z.

4. CONCLUSIONS

In this paper we have demonstrated the ability of CAVEAT to solve a selection of hydrodynamics test problems. First-order, second-order, and rezoned versus Lagrangian solutions were compared. The solutions were obtained using a three-dimensional version of the code that uses a Godunov method with an approximate Riemann solver. Although CAVEAT permits periodic or continuous rezoning as an

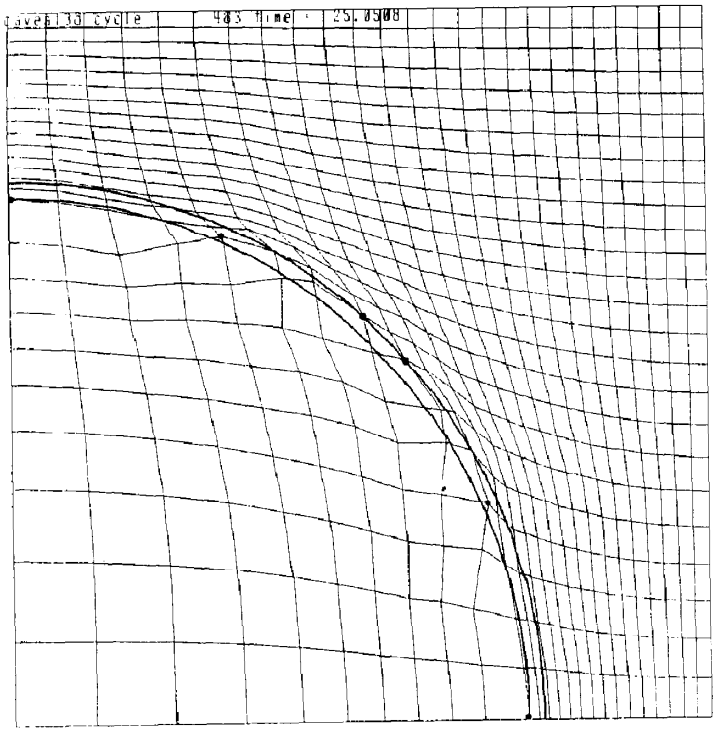

FIG. 27. The indicated points have the same densities. The curves drawn on the mesh are quarter-circles centered at the origin.

option, rezoning was avoided where it would simplify the problem, as in the case of the Saltzman piston problem. There were few surprises in the results: rezoning was found to result in diffusive errors of the type encountered in Eulerian solutions, first-order solutions were smoother, and second-order solutions were more accurate.

ACKNOWLEDGMENTS

The author thanks the people of T-3 group at Los Alamos National Laboratory, and in particular John Baumgardner, for their continuing help. In addition, the author thanks Len Margolin of Lawrence Livermore National Laboratory, for suggesting several of the test problems and John Bolstad of Lawrence Livermore National Laboratory, for suggesting that this work be published.

REFERENCES

1. J. DUKOWICZ, *J. Comput. Phys.* **61**, 119 (1985).
2. F. L. ADDESSIO, D. E. CARROLL, J. K. DUKOWICZ, F. H. HARLOW, J. N. JOHNSON, B. A. KASHIWA,

M. E. MALTRUD, AND H. M. RUPPEL, Los Alamos National Laboratory Report LA-10613-MS, 1986 (unpublished).
3. J. U. BRACKBILL AND J. S. SALTZMAN, *J. Comput. Phys.* **46**, 342 (1982).
4. J. SALTZMAN AND P. COLELLA, manuscript in preparation (1987).
5. P. COLELLA, *SIAM J. Sci. Statist. Comput.* **3**, 76 (1982).
6. J. VON NEUMANN AND R. D. RICHTMYER, *J. Appl. Phys.* **21**, 232 (1950).
7. R. LANDSHOFF, Los Alamos Scientific Laboratory Report LA-1930, 1955 (unpublished).
8. W. F. NOH, Lawrence Livermore National Laboratory Report UCRL-53669, 1985 (unpublished).
9. P. WOODWARD AND P. COLELLA, *J. Comput. Phys.* **54**, 115 (1984).